A Numerical Analysis of the Tensile Test for Sheet Metals

AMIT K. GHOSH

The strain hardening, strain-rate hardening, and plastic anisotropy properties of metal sheets are normally determined in a tensile test during the nearly uniform deformation prior to the maximum load. Beyond this point, strain nonuniformity leading to a neck is poorly understood in terms of interaction of these material properties with changes in strain-rate and stress-state within the neck, and the resulting load-extension plot. Satisfactory modeling of this problem has been achieved by using a rigid/plastic constitutive law including strain hardening and strain-rate hardening. Progressive cessation of deformation starting from elements in the specimen fillet region toward the center is demonstrated. This effect is shown to generate a strain peak (neck) at the gage length center. The predicted load-extension plots and strain distributions in the neck agree well with experiments conducted on a number of test materials. This work provides a quantitative measure of the influence of various material parameters on tensile ductility and identifies the proper constitutive law for input into mathematical models of more complex forming operations.

DURING tensile tests of engineering sheet materials, the records of load *vs* elongation are routinely translated into true stress-true strain curves. These records can be utilized up to the maximum load points, since deformation is practically uniform over the gage length within this load range. In strain hardening metals, true stress-true strain relations are fitted to a power law, $\sigma = K\epsilon^n$, and this relationship is assumed to continue beyond maximum load.

Beyond the maximum load deformation becomes nonuniform, and gage length elongations can no longer be used to obtain true strain or true stress in the deforming element. In a specimen of strain-hardening material containing an imperfection (*e.g.*, variation in cross sectional area) once the maximum load for the imperfection site is attained, a simple one-dimensional model suggests that all other material elements in the specimen would stop deforming; since this site can now continue to deform under a falling load. This further suggests negligible post-uniform* extension over the gage length. However the facts are that the imperfection site does not deform by itself and that the strain concentration is spread over the neighboring elements. The strain nonuniformity so developed is thus gradual and not of a step-function nature as assumed in many investigations. In the present paper a pseudotwo-dimensional analysis of plastic deformation has been made with realistic strain gradients accompanying the development of a neck.

*In this paper, the term uniform elongation refers to strain at maximum load, while post-uniform extension is the elongation after maximum load. All elongations reported here are for a 50.8 mm gage length.

It is known that uniform elongation is directly related to the strain hardening exponent, n, while the post-uniform deformation is controlled by strain-rate sensitivity, m (as in the hardening law: $\sigma = K\epsilon^n\dot{\epsilon}^m$), as the strain-rate gradients in the specimen become significant.[1-3] In addition, since the stress-state in the developing neck deviates from uniaxial tension, the plastic anisotropy parameter, r (the ratio of width-to-thickness strain) which influences the local flow stress, also affects the post-uniform extension.[1,2]

The relationship between these phenomenological parameters and tensile elongation has been only semi-quantitatively defined until now.[1-4] Analytical predictions of strain-distribution, and in particular, triaxial stresses have been made (with the help of finite element methods[5,6]) only for round tensile specimens of elastic-plastic, strain hardening materials. The latter study was related to the initiation of ductile fracture,[6] and not to the overall load-extension characteristics in a tensile test. Moreover, none of these works incorporate the influence of strain-rate sensitivity. While stress triaxiality may be ignored for sheet specimens, the strain-rate sensitivity and the effect of the intermediate principal stress cannot be. The present analytical model for the tensile test relates numerical results on load, extension and neck development to phenomenological inputs, thereby providing a better understanding of this widely-used engineering test.

ANALYSIS

We begin with a specimen which has developed a nonuniform geometric profile under applied load. The nonuniformity has been highly exaggerated for illustrative purposes in Fig. 1(*a*). Cartesian coordinates are located with the origin at the center of the minimum cross section, x-axis along the specimen axis, y-axis along the specimen width, and the z-axis in the thickness direction. Shown in Fig. 1(*b*) are photographs of actual sheet specimens with 0.5 mm square grid printed on the surface to represent the x and y coordinates. During deformation this grid transforms into curvilinear trajectories also shown

AMIT K. GHOSH, formerly with Research Laboratories, General Motors Corporation, Warren, MI is now a Member of the Technical Staff, Science Center, Rockwell International, Thousand Oaks, CA 91360.

Manuscript submitted September 29, 1976.

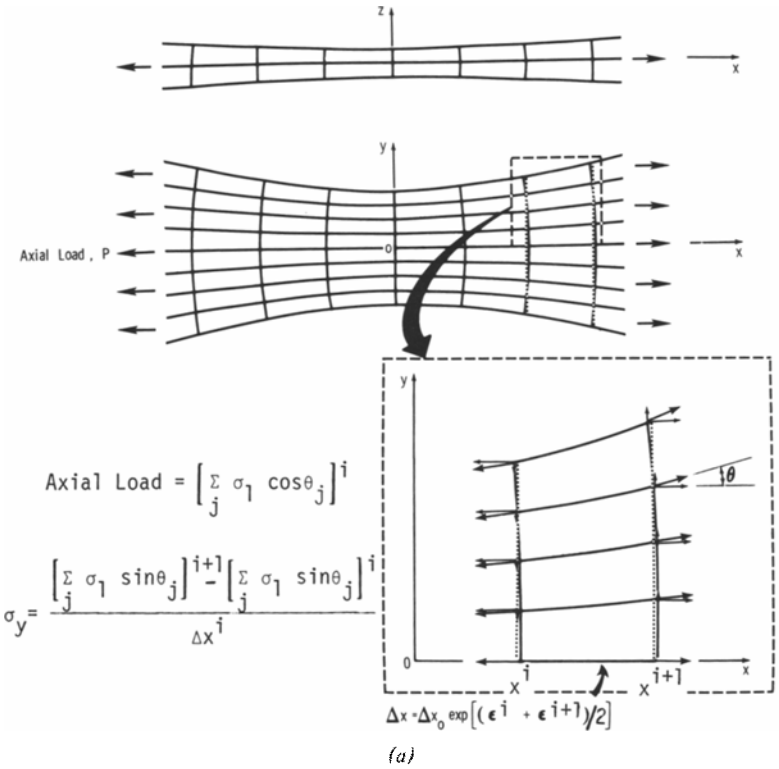

(a)

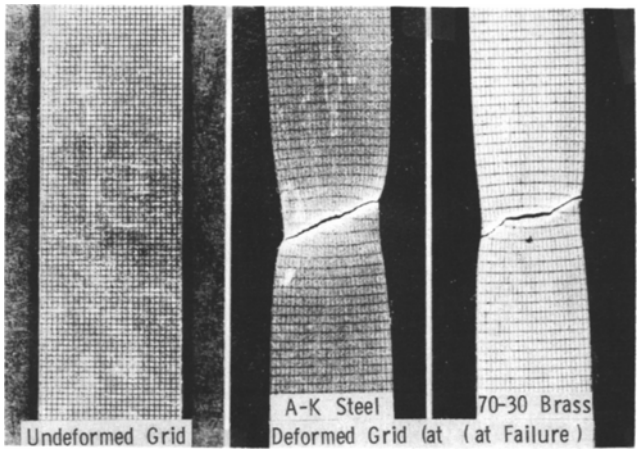

(b)

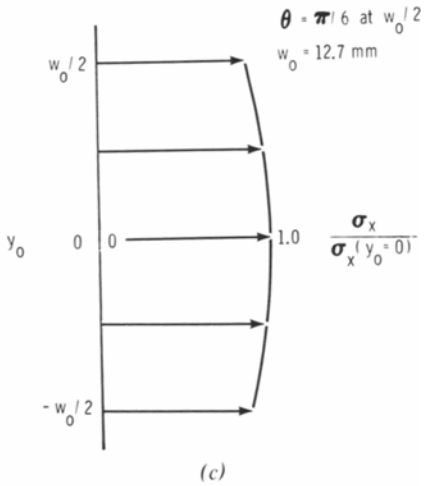

(c)

Fig. 1—(*a*) Nonuniformity developed during deformation of a sheet tensile specimen is highly exaggerated in two sectional views. Stress, σ_1, acts along trajectories (shown in the inset), the sum of whose components in the x-direction support the axial load. The curvilinear nature of y and z lines is ignored and is replaced by straight lines, shown dashed. (*b*) An undeformed photogrid (0.5 mm square) on a tensile specimen is contrasted with the deformed grid on brass and steel specimens at failure. Except for the failure region, most of the specimen exhibits near-linear behavior of y-lines, as in the schematic representation of Fig. 1(*a*). Figure 1(*c*) shows axial stress (σ_x) distribution across the width according to the present model, showing the greatest axial stress along the central axis and a decrease toward the specimen edges.

here and schematically illustrated in Fig. 1(*a*). The trajectories are mutually orthogonal and represent the directions of principal stress and strain. The width strain measured from the specimens has been found to be extremely uniform across the specimen width at any x. This fact provides an important starting point for the present analysis. For very wide specimens, however, in which the stress system deviates from uniaxial, this assumption may not be expected to hold.

A critical feature of a specimen possessing a gradient in cross sectional area is that only the area sum of the x-components of the trajectory stresses (σ_1) at each cross section will have to equal the axial load, P. Consequently, σ_1 along the curvilinear trajectories could be larger than the average axial stress, σ_x. For sufficiently large strain gradients, as would occur if a neck is well developed, the stress along the trajectory would be sufficient to cause deformation in elements away from the minimum cross section site even under a falling load.

To relate trajectory strain ϵ_1 to axial strain ϵ_x, we first recall that the width strain is found to be uniform at any x, which means that ϵ_1 is fixed at any x for all trajectories. Secondly, the curvatures of y-lines are so slight even at fracture (see Fig. 1(*b*)), that they can be assumed to be straight for the purpose of computing axial strain. In Fig. 1(*a*), these assumed y lines are indicated by dashed lines at average x positions. This implies $\epsilon_1(x) = \epsilon_x(x)$, which in terms of original coordinate position, x_0, means $\epsilon_1(x_0) = \epsilon_x(x_0)$. The uniformity of $\epsilon_1(x)$ also implies uniformity of trajectory stress, $\sigma_1(x)$, throughout each cross section, the only variation being in the angle of its application as functions of y and z. Figure 1(*c*) shows that this permits the axial stress component (of σ_1) to be greatest along the x-axis and to decrease toward the edges. This is con-

sistent with previous calculations[5,7] of stress distribution in a tensile neck. Thus the axial load, $P(x)$ is given by

$$P(x) = 4 \int_{z=0}^{t/2} \int_{y=0}^{w/2} \sigma_1(x) \cos\theta \cos\phi \, dy \, dz \qquad [1]$$

where $\sigma_1(x)$ makes an angle ϕ with the x-y plane, while its projection on the x-y plane makes an angle θ with the x-axis; w and t are, respectively, the current width and thickness at x.

In terms of the original ccordinate positions x_0, y_0 and z_0, the strain uniformity across the width (and therefore thickness) implies

$$y = y_0 e^{\epsilon_2(x_0)} = y_0 e^{\epsilon_y(x_0)} \qquad [2a]$$

$$z = z_0 e^{\epsilon_3(x_0)} = z_0 e^{\epsilon_z(x_0)} \qquad [2b]$$

where ϵ_2 and ϵ_3 are the width and thickness strains along the trajectories, and ϵ_y and ϵ_z are the width and thickness strains along the principal axes (y and z). Again, since $dx = dx_0 e^{\epsilon_x(x_0)}$, $\cos\theta$ and $\cos\phi$ in Eq. [1] can be determined from the following expressions which are obtained by differentiating Eqs. [2a] and [2b] with respect to x:

$$\tan\theta = \frac{dy}{dx} = \left\{ \frac{1}{y_0}\frac{dy_0}{dx_0} + \frac{d\epsilon_y}{dx_0} \right\} y_0 e^{\epsilon_y - \epsilon_x} \qquad [3]$$

and

$$\tan\phi = \frac{dz}{dx} = \left\{ \frac{1}{z_0}\frac{dz_0}{dx_0} + \frac{d\epsilon_z}{dx_0} \right\} z_0 e^{\epsilon_z - \epsilon_x}. \qquad [4]$$

If $\tan\theta$ and $\tan\phi$ are known at any stage during deformation, and since $\sigma_1(x_0)$ is independent of y_0 and z_0 at any x_0, Eq. [1] can be written in terms of x_0 as

$$P(x_0) = 4\,\sigma_1(x_0) \int_0^{w/2} \frac{dy}{\sqrt{1 + A^2 y_0^2}} \int_0^{t/2} \frac{dz}{\sqrt{1 + B^2 z_0^2}} \qquad [5]$$

where $A = \{(1/y_0)(dy_0/dx_0) + (d\epsilon_y/dx_0)\} e^{\epsilon_y - \epsilon_x}$ and $B = \{(1/z_0)(dz_0/dx_0) + (d\epsilon_z/dx_0)\} e^{\epsilon_z - \epsilon_x}$. Now, using derivative of Eqs. [2a] and [2b] and the law of volume constancy in Eq. [5], axial load becomes

$$P(x_0) = 4\,\sigma_1(x_0)\, e^{-\epsilon_x(x_0)} \int_0^{w_0/2} \frac{dy_0}{\sqrt{1 + A^2 y_0^2}} \int_0^{t_0/2} \frac{dz_0}{\sqrt{1 + B^2 z_0^2}}, \qquad [6]$$

Upon integration Eq. [6] becomes

$$P(x_0) = \frac{4\,\sigma_1(x_0)\, e^{-\epsilon_x(x_0)}}{AB} \{\sinh^{-1}(Aw_0/2) \sinh^{-1}(Bt_0/2)\}. \qquad [7]$$

As θ and ϕ approach zero, *i.e.*, when the gradient is negligible, $(1/A)\sinh^{-1}(Aw_0/2)$ and $(1/B)\sinh^{-1}(Bt_0/2)$ reduce respectively to $w_0/2$ and $t_0/2$, and axial load has the familiar form: $P(x_0) = (w_0 t_0)\, e^{-\epsilon_x(x_0)} \sigma_1(x_0)$. Since the minimum section at $x = x_0 = 0$ is likely to have zero gradient (particularly if the specimen is symmetric about $x = 0$), the axial load on the specimen at any instant is given by

$$P = (w_0 t_0)\, e^{-\epsilon_x(0)} \sigma_1(0). \qquad [8]$$

Thus both Eqs. [7] and [8] are obtained in terms of the trajectory stress, σ_1. The solution for $\epsilon_x(x_0)$ at any time now requires satisfying the load equilibrium condition: $P(x_0) = P$, provided proper account is taken of the departure of the stress-state from uniaxiality, while computing $\sigma_1(x_0)$.

Principal Stresses and Stress-Ratio

The departure from uniaxiality of stress in each element is handled by determining the average principal stresses in x, y and z directions which are subsequently used in calculating effective stress. Since each element is treated as a unit, the principal stress in the x-direction is obtained by dividing the axial load from Eq. [7] by the cross sectional area, $(w_0 t_0)\, e^{-\epsilon_1(x_0)}$. Thus

$$\sigma_x(x_0) = \left\{ \sinh^{-1}\left(\frac{Aw_0}{2}\right) \Big/ \left(\frac{Aw_0}{2}\right) \right\} \times \left\{ \sinh^{-1}\left(\frac{Bt_0}{2}\right) \Big/ \left(\frac{Bt_0}{2}\right) \right\} \sigma_1(x_0). \qquad [9]$$

The intermediate and through-thickness stresses (σ_y and σ_z, respectively) are obtained from considering the sum of y- and z-components of σ_1, respectively. Since body forces are absent in y and z directions, σ_y and σ_z could be obtained by differentiating the sum of y- and z-components with respect to x. Neglecting σ_z for sheet specimens,* σ_y can be expressed by

*Since $\sigma_z(x_0)$ is rather small for thin sheets until the stage of a through-thickness neck formation, it will be excluded from the present analysis.

$$\sigma_y(x) = \frac{d}{dx}\left[\int_0^{w/2} \sigma_1(x_0) \sin\theta \, dy \right]. \qquad [10]$$

Now substituting $dx = dx_0 e^{\epsilon_x(x_0)}$, $dy = dy_0 e^{\epsilon_y(x_0)}$ and $\sin\theta = (Ay_0/\sqrt{1 + A^2 y_0^2})$, Eq. [10] can be expressed in terms of the original coordinates as

$$\sigma_y(x_0) = \frac{d}{dx_0}\left[\sigma_1(x_0)\, e^{\epsilon_y - \epsilon_x} \int_0^{w_0/2} \frac{Ay_0 dy_0}{\sqrt{1 + A^2 y_0^2}} \right] \qquad [11]$$

which can be further simplified to

$$\sigma_y(x_0) = \frac{d}{dx_0}\left[\sigma_1(x_0)\, e^{\epsilon_y - \epsilon_x} \left\{ \frac{\sqrt{1 + A^2 w_0^2/4} - 1}{A} \right\} \right]. \qquad [12]$$

The principal stress-ratio, $[\sigma_y(x_0)/\sigma_x(x_0)]$, needed for computing effective stress and strain-rate ratio in the next section, is obtained by dividing Eq. [12] by Eq. [9].

Formulation of the Incremental Problem

A constitutive law describing effective stress $\bar{\sigma}$ in terms of effective strain $\bar{\epsilon}$ and effective strain rate $\dot{\bar{\epsilon}}$ is required as input for the present problem. Two principal assumptions are used according to continuum plasticity theory in order to relate effective stress and strain-rate to axial stress and strain rate. These are: i) planar isotropy in the sheet, with the presence of normal anisotropy, r, and ii) isotropic hardening, *i.e.* uniform expansion of the Hill-modified anisotropic yield surface. Based on these assumptions, the effective stress is given by

$$\bar{\sigma} = \sqrt{\frac{3(1 + r)}{2(2 + r)}} \left\{ 1 + \alpha^2 - \frac{2r\alpha}{1 + r} \right\}^{1/2} \sigma_x \qquad [13]$$

where α = stress-ratio (σ_y/σ_x); the effective strain-rate is given by

$$\dot{\bar{\epsilon}} = \sqrt{\frac{2(1+r)(2+r)}{3(2r+1)}} \left\{1 + \rho^2 + \frac{2r\rho}{1+r}\right\}^{1/2} \dot{\epsilon}_x \qquad [14]$$

where ρ = strain-rate ratio ($\dot{\epsilon}_y/\dot{\epsilon}_x$); and finally a modified form of the associated flow rule is given by

$$\alpha = (\sigma_y/\sigma_x) = \frac{(1+r)\rho + r}{1 + r + r\rho}. \qquad [15]$$

If $\rho(x)$ is known at a certain instant during deformation, $\alpha(x)$ can be obtained from Eq. [15], and substituted in Eq. [13] to express $\sigma_x(x)$ in terms of $\bar{\sigma}(x)$. The trajectory stress, $\sigma_1(x)$ can then be expressed in terms of $\bar{\sigma}(x)$ with the use of Eq. [9]. If both $\rho(x)$ and $\dot{\epsilon}_x(x)$ are known as functions of time, integration of Eq. [14] with respect to time gives the effective strain,

$$\bar{\epsilon}(x) = \sqrt{\frac{2(1+r)(2+r)}{3(2r+1)}} \int_0^t \left\{1 + \rho^2(x,t) + \frac{2r\rho(x,t)}{1+r}\right\}^{1/2} \times \dot{\epsilon}_x(x,t)dt. \qquad [16]$$

From these two steps, $\sigma_1(x)$ can be expressed in terms of $\rho(x)$ and $\dot{\epsilon}_x(x)$ with the use of a proper constitutive equation relating $\bar{\sigma}(x)$ to $\bar{\epsilon}(x)$ and $\dot{\bar{\epsilon}}(x)$. This $\sigma_1(x)$ can then be substituted in Eq. [7], while $\epsilon_x(x)$ in Eq. [7] is determined from the integration:

$$\epsilon_x(x) = \int_0^t \dot{\epsilon}_x(x,t)dt.$$

The present method of solution for $\epsilon_x(x,t)$ is based on a quasi-static approach in which a fixed strain increment, $\Delta\epsilon_x(0)$, is assigned at the minimum cross section during each step, and corresponding solutions for $\Delta\epsilon_x(x)$ or $\dot{\epsilon}_x(x)$ are found that satisfy the equilibrium equation: $P = P(x)$. With initial $\rho(x)$ and $\dot{\epsilon}_x(0)$ as inputs, successive solutions for $\epsilon_x(x,t)$ allow updating of $\rho(x,t)$ and $\dot{\epsilon}_x(x,t)$. Details of the numerical procedure are given later.

Constitutive Law

Most engineering materials exhibiting strain-rate sensitivity at room temperature can be approximately described by a constitutive law in which strain rate hardening term is additive to the strain hardening term. Such a law is given by[1]

$$\bar{\sigma} = K[\bar{\epsilon}^n + m \ln(\dot{\bar{\epsilon}}/\dot{\epsilon}_0)] \qquad [17a]$$

where $\bar{\sigma}$ = effective stress, $\bar{\epsilon}$ = effective strain, $\dot{\bar{\epsilon}}$ = effective strain-rate, $\dot{\epsilon}_0$ = reference strain-rate, K = strength coefficient, n = strain hardening exponent, m = strain-rate hardening index. A very slow rate (*e.g.* 0.003 s^{-1}) is chosen as the reference strain-rate in this work. As long as Eq. [17a] describes the material behavior for the strain-rates of interest, the choice of this parameter ($\dot{\epsilon}_0$) has little effect on the calculation. This equation has been used in most of the calculations in this paper.

A second constitutive law, expressed as the product of the strain hardening and strain-rate hardening terms and often quoted in the literature, is given by:

$$\bar{\sigma} = K\bar{\epsilon}^n \dot{\bar{\epsilon}}^{m'}. \qquad [17b]$$

This strain-rate hardening exponent, m', is different from the previous value m. For the same flow-stress-differential, $\Delta\sigma$, between two strain-rates, m' is slightly larger than m. While some objections can be raised to Eq. [17b], it applies somewhat better to deformation at elevated temperature and a limited number of calculations have been made using it.

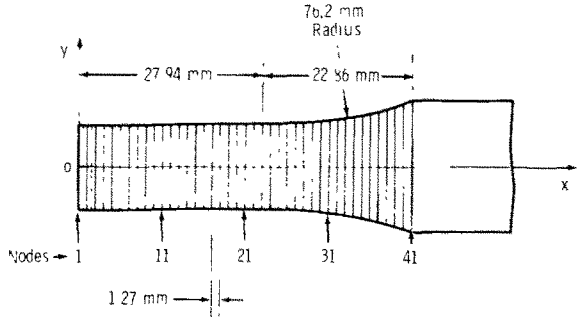

(a)

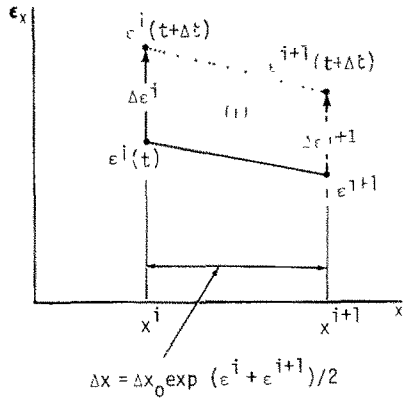

$$\Delta x = \Delta x_0 \exp\left(\epsilon^i + \epsilon^{i+1}\right)/2$$

(b)

Fig. 2—(*a*) One-half of an E-8 sheet tensile specimen has been divided into 40 equal elements (41 nodes). This half covers 27.94 mm of straight central section and 22.86 mm of radiused fillet region. The central 25.4 mm of the straight section belongs to the gage length (50.8 mm), over which extension is measured. To provide sufficient accuracy, the first two elements are subdivided into two more elements. (A constant crosshead speed is maintained between the 1st and the 41st nodes.) (*b*) Graphical representation of the iterative scheme for calculating the strain increment at the $(i+1)$th node when the same is known at the ith node. Linearity of ϵ_x within each element is assumed. The various quantities for the equilibrium equation have been developed.

NUMERICAL COMPUTATION

General Procedure

A finite difference procedure was used for computation of $\epsilon_x(x, t)$ along the specimen length at each time step. The length (between grips) of an ASTM standard E-8 specimen (101.6 mm) was divided into 80 equal elements, each 1.27 mm long, along the x-direction. (The central 55.88 mm has uniform cross section, and the fillet radii near the ends cover the rest of the specimen.) Since the specimen is symmetric about $x = 0$ only one-half is considered (Fig. 2(a)), with the first node at $x = 0$ and the 41st node at $x = 50.8$ mm. Experiments with smaller size elements proved to be unnecessary, while elements as coarse as 3 mm may even be adequate. To provide adequate capability for strain localization during the formation of a neck, the two central elements (on either side of $x = 0$) were further subdivided equally, as shown in Fig. 2(a). A constant displacement rate (crosshead speed, S) was maintained across the original length of 101.6 mm. Additional calculations with the same crosshead speed applied only across the gage length (50.8 mm), produced little difference in the load-elongation characteristics and hence are excluded from further discussion.

During each time increment (between t and $t + \Delta t$), ϵ_x is incremented by a constant amount (0.01) at $x = 0$, and $\epsilon_x(x)$ is calculated throughout the specimen. Strain, ϵ_x, is assumed to be a linear function of x within each element. The graphical representation in Fig. 2(b) shows that if strain is known at all node positions at time t, and if $\Delta\epsilon_x$ is known at the ith node, the problem is one of finding $\Delta\epsilon_x$ at $(i + 1)$th node. The strain increment in the ith element is taken as the average of those at the bounding nodes (ith and $(i + 1)$th), while the strain gradient is determined by dividing the node strain difference by the current node separation, $\Delta x^{(i)} = \Delta x_0 \exp\left[1/2\{\epsilon_x^i(t + \Delta t) + \epsilon_x^{i+1}(t + \Delta t)\}\right] = \Delta x_0 \exp\left[1/2\{\epsilon_x^i(t) + \epsilon_x^{i+1}(t) + \Delta\epsilon_x^i + \Delta\epsilon_x^{i+1}\}\right]$. The unknown quantity, $\Delta\epsilon_x^{i+1}$, is determined by equating axial load carried by the ith element with that at $x = 0$, as discussed before. A simple Newton-Raphson iterative scheme is found adequate for the solution. Starting from $i = 1$, progressive solutions are thus made for each element, with $\epsilon_x^i(t + \Delta t)$ serving as the input for finding $\epsilon_x^{i+1}(t + \Delta t)$.

Once $\epsilon_x(x)$ is known for all nodes at $t + \Delta t$, the current length is computed by integrating over all elements, $\Delta x^{(i)}$, and the length increment is determined by subtracting the length before the step. From the known crosshead speed, the time increment, Δt, necessary for the length increment is calculated. (Since $\Delta\epsilon_x$ at $x = 0$ is fixed, this time increment is not fixed and self-adjusting in nature.) The incremental strain-rate $(0.01/\Delta t)$ at $x = 0$ is used for the next time step. The incremental stress- and strain-ratios (α^i and ρ^i) are also calculated at the end of each step from the current values of ϵ_x^i and $(d\epsilon_x/dx)^{(i)}$ using Eqs. [9], [12], and [15], and used as input for the next Δt. The iterative solution procedure is then repeated and a new $\epsilon_x(x)$ is developed. The specimen elongation in terms of engineering strain is computed for the central 40 elements (*i.e.* over 50.8 mm gage length) at each stage by a separate integration scheme. The value of the axial load is also computed at each stage and load *vs* engineering strain plots are shown later on in this paper.

Initialization

The solution procedure was started by assigning $\epsilon_x^i = 0$, $\alpha^i = 0$, and $\rho^i = -R/(1 + R)$ for all i. This value of ρ^i follows from Eq. [15] under uniaxial stress state. Beginning with the first time step, $\Delta\epsilon_x^1$ (at the center of the specimen) is chosen to be equal to 0.01.* Based on the uniform central section of 55.88 mm the initial strain rate would be $S/55.88$ s^{-1}, while using the entire sample length it is $S/101.6$ s^{-1}, where S = crosshead speed in mm/s. An average of these two rates is used as the initial strain rate at $x = 0$. At the end of the first step the program calculates the appropriate strain-rate, ρ^i and α^i for the next step. This procedure of using a strain increment at $x = 0$ is somewhat arbitrary for specimens with no imperfection; however, it is quite reasonable when a small imperfection is situated at the center of the specimen.

*Experiments with small strain increments did not produce any better accuracy, while larger strain increments proved to be too coarse.

Specimen Imperfection

All imperfections are assumed to be geometric and the material, itself, is treated as perfectly homogeneous. The role of inclusions and other material inhomogeneities are neglected for the present calculations since their micromechanics is quite complicated, and in many ductile metals their role on flow localization may not be significant. Engineering tests are normally performed with specimens having a slight width taper toward the center (*e.g.*, center width ~0.005 mm less than that near the fillet), which was simulated by a cosine-wave type width variation within the central 55.88 mm (Fig. 3). This type of imperfection allows smooth slopes at $x = 0$ and at $x = 27.94$ mm. Calculations were carried out for a number of imperfection size parameters, $f = (\Delta w/w_0)$. Additional calculations were made for a half cosine-wave imperfection over the gage length only, ignoring specimen fillet, a localized full cosine-wave imperfection over the central 10.16 mm, and no imperfection at all.

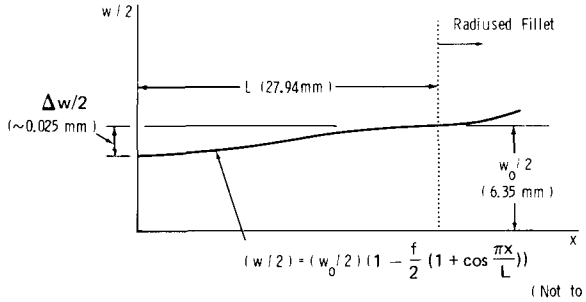

Fig. 3—A schematic representation of the cosine-wave type imperfection in the specimen width dimension. Semi-wave length is 27.94 mm, which is equal to the straight section of Fig. 2(a), beyond which the fillet radius starts. The above cosine equation for the straight section and a quadratic equation for the fillet section are used to calculate w_0 for input into Eq. [7].

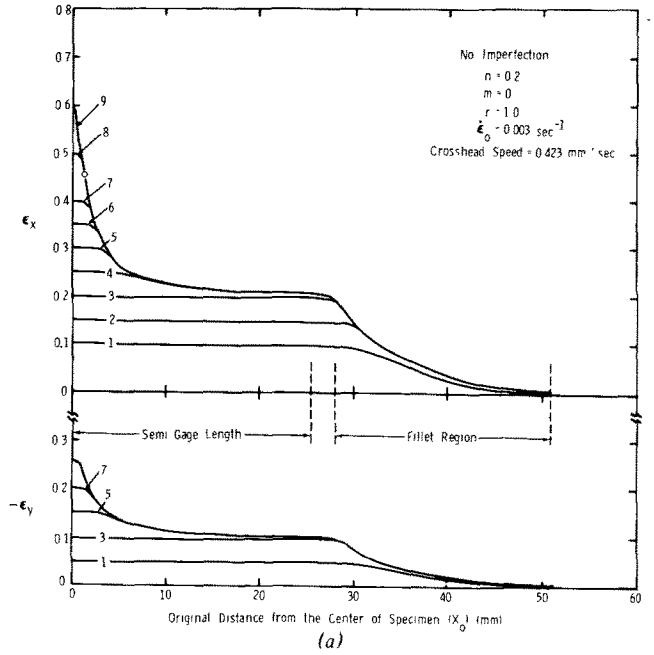

(a)

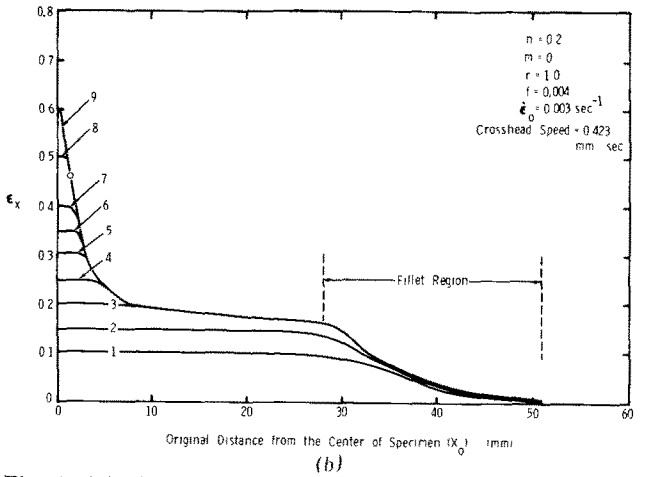

(b)

Fig. 4—(*a*) Distributions of axial and transverse strains in a perfect tensile specimen as functions of original distance from the center at different stages of deformation. Calculation has been carried out with (m = 0). Note that strain within the straight section is uniform, when $\epsilon_x \leq 0.2$. The open circle indicates a node that is 1.27 mm from specimen center, the deformation within which may be somewhat inaccurately predicted. (*b*) Distributions of axial strain in a tensile specimen on functions of original distance from the center, at different stages of deformation of a specimen with imperfection size ($\Delta w/w_0$) of 0.004. Note that deformation within the straight section becomes nonuniform even below ϵ_x = 0.2. (*c*) Distributions of stress-ratio (σ_y/σ_x) as functions of original distance from the center, at several stages of deformation, for a perfect specimen with n = 0.2, m = 0.01 and r = 1. The stages of straining are indicated by noting the value of peak strain on each distribution.

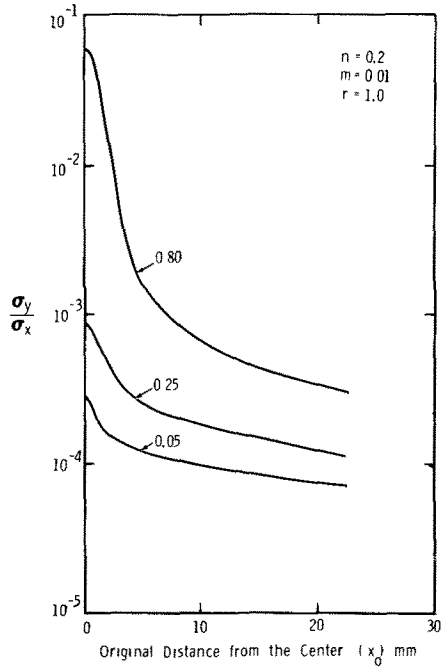

(c)

Fig. 4—Continued.

Discontinuance of Straining

Since the quasi-static solutions are made incrementally, a node with $\Delta\epsilon_x^i \leq 0$ during a certain step may find suitable strain and strain-rate increments later to permit $\Delta\epsilon_x^i > 0$. However, such solutions should be allowed only while the load is still rising. Thus if the load increment in the last step has been negative and $\Delta\epsilon_x^i \leq 0$, all nodes between i and 41 are considered inoperative. If the load increment has been positive and yet $\Delta\epsilon_x^i \leq 0$, all nodes between i and 41 remain at their previous strain values. This mechanism allows the development of a strain peak by discontinuance of deformation through successive elements, particularly during unloading of the specimen. Eventually only the central node keeps on deforming and the computation procedure is terminated when it reaches the fracture strain.

NUMERICAL RESULTS AND DISCUSSIONS

The results of computation provide general information on strain and stress distributions along the axial and transverse directions in the specimen, the influence of the imperfection parameter, f, the influences of material parameters, n, m and r and the engineering stress-strain curves. The fracture strain is chosen somewhat arbitrarily for the parameter study. However, if fracture strain is large, small variations in it do not seem to have any significant influence on the tensile elongations measured over 50.8 mm gage length.

Figure 4(*a*) shows incremental axial and transverse strains as functions of x_0 for the case of n = 0.2, m = 0, and r = 1.0 in a specimen without imperfection. The main features are: i) gage length strain is essentially uniform (variation <0.0002), ii) there is a very gradual decay toward the fillet, and iii) an exponential drop-off within the fillet region. During deformation, the strain level increases in all regions, however, the strain nonuniformity within the gage length increases as the "knee" between gage length and fillet strain distributions moves closer to the specimen center. At Stage 3, the "knee" has already moved into the central 55.88 mm (which originally had uniform cross section), and fillet strain stops

increasing. Subsequently, straining progressively discontinues in elements approaching the specimen center and leads to the dynamic development of a strain peak. Thus the constraints imposed by greater cross sectional areas in the fillet force the development and growth of a strain nonuniformity in an otherwise perfect specimen.

A small cosine imperfection ($f = 0.004$) produces an appreciable strain nonuniformity much earlier during deformation (Fig. 4(*b*)), thereby leading to premature discontinuance of deformation in most elements of the gage length. This results in an early development of strain peak and a smaller uniform strain. Thus ϵ_x cannot become greater than n as long as there is an imperfection within the gage length.

The stress-ratio (σ_y/σ_x) distribution in the specimen is shown in Fig. 4(*c*). For most of the deformation history, this remains very small ($\sim 10^{-4}$). More rapid increase takes place near $x_0 = 0$, and rises almost up to 10^{-1} when all but a couple of central elements have stopped deforming. It is clear that the thickness gradient becomes sufficiently large at this stage that the effects from σ_z/σ_x should also be considered in calculating effective stresses. Since this is ignored in the present paper, the amount of deformation beyond this point is somewhat underestimated. The strain distributions and load-elongation plots to be presented subsequently are marked by a closed circle to indicate this point. With reference to the metal forming literature, this strain would be very close to the strain limit at the onset of a localized thickness neck (forming limit).*

*It may be noted that during gradual strain localization within the diffuse neck a condition of oblique localized necking (due to R. Hill *J Mech. Phys. Solids*, vol. 1, 1952, p. 19) may be satisfied for certain materials. This condition can be incorporated with the present analysis for a more complete picture, however this would neither alter the total elongation nor forming limit appreciably In fact, when the deforming zone of metal shrinks to the size of sheet thickness, the localized strain levels from the current analysis are in good agreement with experimentally observed forming limits

The tensile strain rate ($\dot{\epsilon}_x$) in different elements varies over several orders of magnitude during a test at constant crosshead speed. Figures 5(*a*) and (*b*) show the strain rate in various elements as a function of ϵ_x at the center. The strain-rate at $x_0 = 0$ is found to increase continuously from the start of deformation, contrary to what might have been expected from the specimen elongation. The reason for this lies in the drop in $\dot{\epsilon}_x$ in other elements, thereby forcing a greater deformation rate at $x_0 = 0$. For $n = 0.2$ and $m = 0$ (Fig. 5(*a*)), two distinctly different regimes of ϵ_x are observed for $\dot{\epsilon}_x$ at $x = 0$. The sharp rise in $\dot{\epsilon}_x$ before $\epsilon_x = n$ is related to discontinuance of deformation in all fillet elements. In the second stage $\dot{\epsilon}_x$ increases at a slower rate initially, however, gradual strain localization leads to a further rapid increase in $\dot{\epsilon}_x$ before fracture. In the case of $n = 0.2$ and $m = 0.01$, the distinct change in deformation modes occurs much beyond $\epsilon_x = n$. In fact, there is a substantial amount of diffusely distributed strain ($0.20 \leq \epsilon_x \leq 0.36$), during which $\dot{\epsilon}_x$ increases with gradually rising slope. All elements in the fillet discontinue to deform at $\epsilon_x \sim 0.36$ leading to a stage of strain localization. The rise in $\dot{\epsilon}_x$ is, however, much more gradual than in the case of m

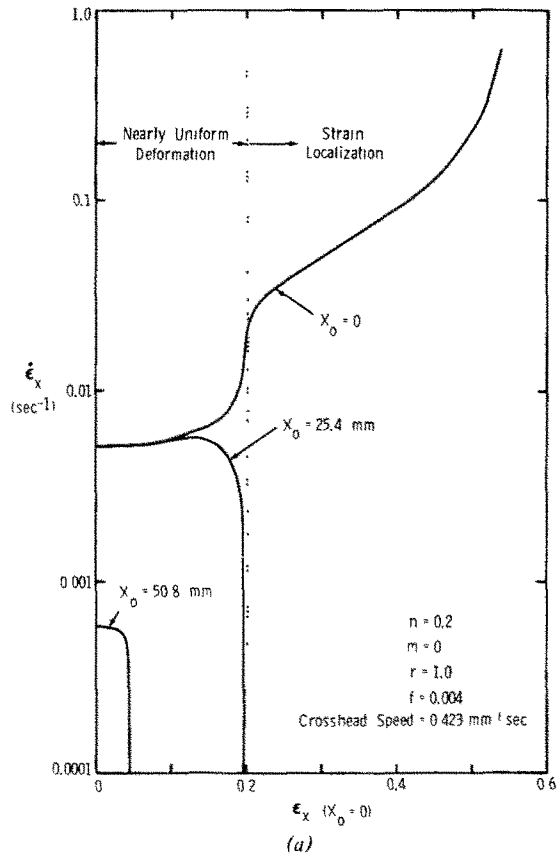

(*a*)

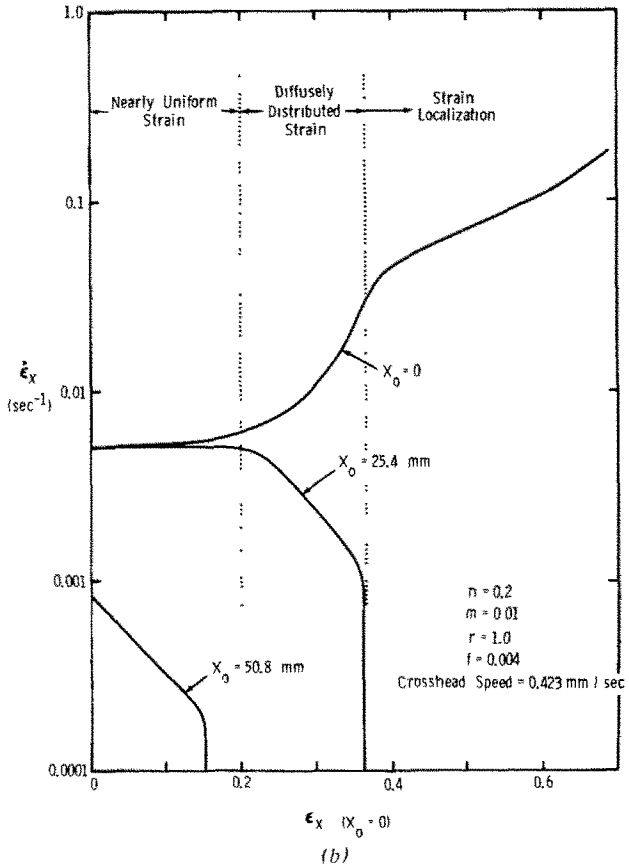

(*b*)

Fig. 5—Axial strain rate, $\dot{\epsilon}_x$, plotted as a function of ϵ_x at $x = 0$ for (*a*) $n = 0.2$ and $m = 0$. (*b*) $n = 0.2$ and $m = 0.01$. The strain rates at three locations on the specimen (each 25.4 mm apart) are shown.

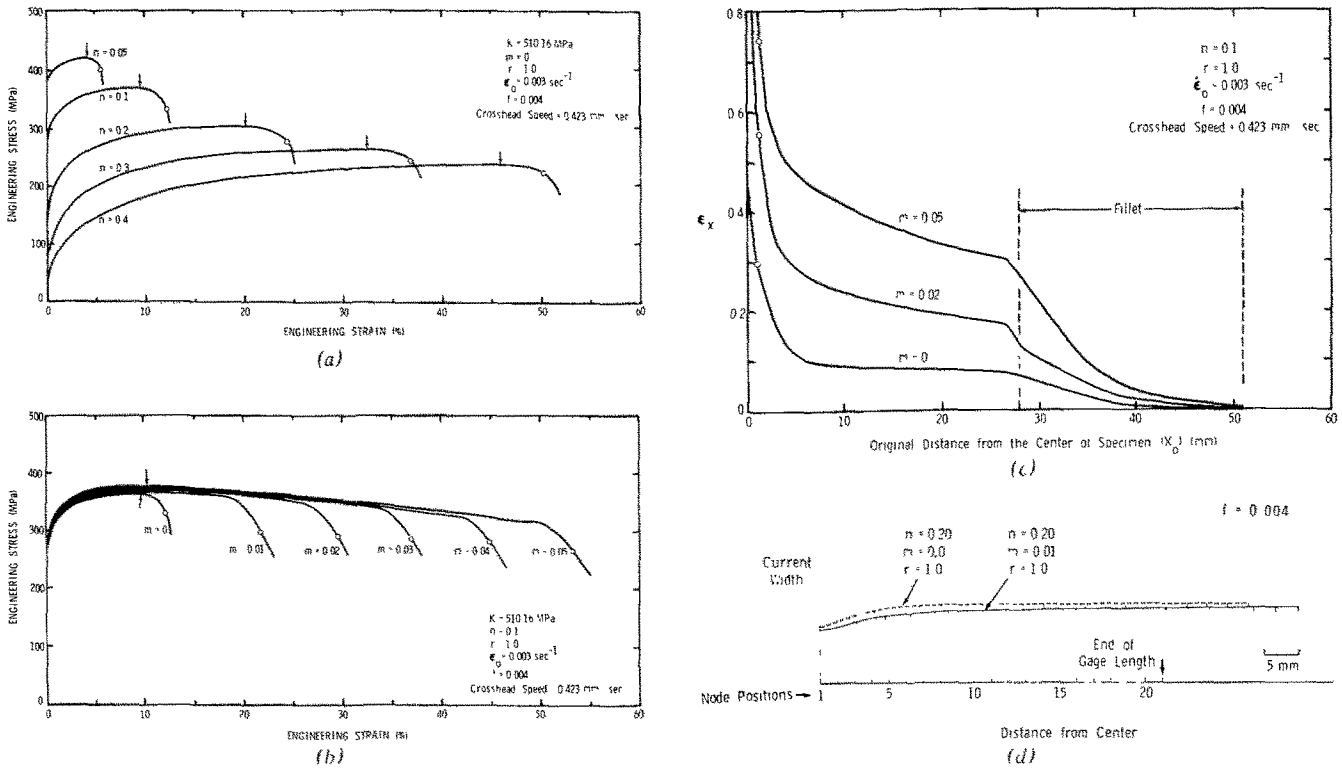

Fig. 6—Engineering stress-strain curves calculated for (*a*) $m = 0$ and an imperfection size (f) of 0.004 for the various values of $n = 0.05$, 0.10, 0.20, 0.30 and 0.40; (*b*) $n = 0.1$ and an imperfection size (f) of 0.004 for the various values of $m = 0$, 0.01, 0.02, 0.03, 0.04 and 0.05. The vertical arrows indicate the maximum load position and the open circles in the decreasing load part of the curves correspond to the discontinuance of deformation at a node 1.27 mm from the specimen center. (*c*) Distributions of axial strain at failure for three different specimens with values of $m = 0$, 0.02 and 0.05 as a function of original distance from center for a fixed value of $n = 0.1$. The open circles indicate a node that is 1.27 mm from specimen center, the deformation within which may be somewhat inaccurately predicted. (*d*) Specimen width profiles for two different specimens, one with $m = 0$ and the other with $m = 0.01$, for nearly identical strains at the specimen center. The extension of the elements is contrasted against the original element size. Note a more diffusely distributed neck for $m = 0.01$, in comparison to the $m = 0$ case.

= 0 (Fig. 5(*a*)). Considerable additional elongation due to this effect has been observed in previous experimental studies[1,2] and is more fully discussed later.

Influence of n

The influence of n on the engineering stress-strain curves is studied for the case of $f = 0.004$, $m = 0$ and $K = 510.16$ MPa (Fig. 6(*a*)), for each of $n = 0.05$, 0.10, 0.20, 0.30 and 0.40. Having the same K for all cases is responsible for the drop in the stress level with increasing value of n. For an imperfection size of 0.004, the uniform strain is always somewhat smaller* than n. As n increases, post-uniform portions of these curves drop more slowly, thereby yielding greater overall strain and suggesting somewhat more stable deformation. Yet, the total strain over 50.8 mm is not much greater than n due to the influence of the imperfection.

*n is in terms of true strains, while specimen extensional strain is expressed in terms of engineering strain.

Influence of m

The influence of m is described in Fig. 6(*b*) for $n = 0.1$, $K = 510.16$ MPa and $\dot{\epsilon}_0 = 0.003$, using the constitutive equation: $\bar{\sigma} = K[\bar{\epsilon}^n + m \ln(\dot{\bar{\epsilon}}/\dot{\epsilon}_0)]$. Engineering stress is raised slightly by an increase in m from 0 to 0.05. The influence of even small values of m (0.01 – 0.05) in extending the post-uniform portion of deformation is quite dramatic and agrees with previous experimental results.[1,2] While the stability of post-uniform deformation increases and the rate of load drop decreases with the rise in m, the uniform strain is affected very little.

This finding contradicts some previous speculations on this subject. The presence of even a small m continues to add deformation throughout the entire gage length (much beyond n) in a quasi-stable manner as illustrated in Fig. 6(*c*). Strain in the fillet region also increases in a similar manner. Note that even though the strain nonuniformity in these plots increases with larger values of m, this would be hardly visible when plotted as a function of instantaneous distance. Figure 6(*d*) shows the instantaneous width plotted as a function of instantaneous length for 1) $m = 0$ and 2) $m = 0.01$, revealing the gradual nature of specimen profile. The wider true neck size is clearly evident even for such a small value of m. This large apparent "uniform" strain may have been responsible for the misconception just cited.

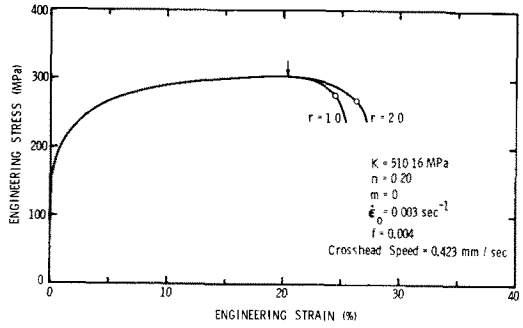

(a)

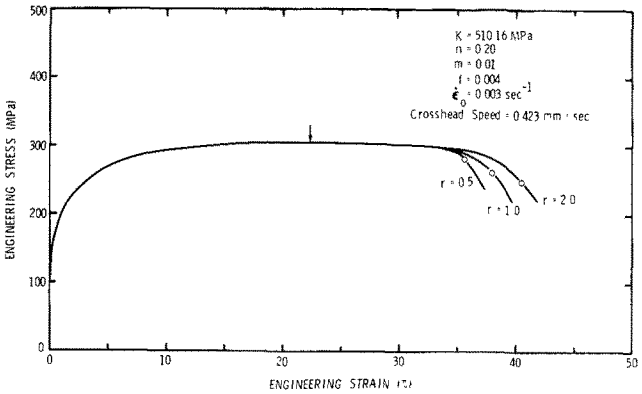

(b)

Fig. 7—Engineering stress-strain curves calculated for (*a*) two different values of r (1.0 and 2.0) for the case of $n = 0.2$ and $m = 0$, (*b*) three different values of r (0.5, 1.0 and 2.0) for the case of $n = 0.2$ and $m = 0.01$. The vertical arrow indicates the maximum load position and the open circles in the decreasing load part of the curves correspond to the discontinuance of deformation at a node 1.27 mm from the specimen center.

Influence of r

The effect of r is shown for two different cases in Fig. 7(*a*) and (*b*). An increase in r increases the post-uniform extension, much like the m-effect. This increase, however, is no more than 2 pct upon raising r from 1.0 to 2.0, for the case of $n = 0.2$, $m = 0$ and $f = 0.004$. For $m = 0.01$ it is a bit larger, as shown in Fig. 7(*b*). A drop in r causes a sharper downtrend for the last part of engineering stress-strain curve and a smaller strain at the onset of a localized thickness neck.

Influence of f

The influence of imperfection size on engineering stress-strain curve is shown in Fig. 8(*a*), for $n = 0.2$, $m = 0$, and $r = 1.0$. Only for a perfect specimen is the uniform strain equal to n, and approximately 6 to 7 pct post-uniform strain achievable. The presence of an imperfection reduces both uniform and post-uniform parts of deformation. For $m = 0.01$, the uniform strain is unaffected by small variations in f (see Fig. 8(*b*)). With no imperfection post-uniform strain in excess of 22 pct is now achievable, however, an increase in imperfection size causes a larger drop in post-uniform strain than that for $m = 0$.

Figure 8(*b*) also shows the influence of a localized cosine-shaped imperfection of $f = 0.002$, spread only over the central 10.16 mm (4 elements on either side of the center) of an otherwise perfect specimen. This localization effect reduces post-uniform strain by as much as 7 pct in comparison to a gradual imperfection of the same size. The uniform strain is not affected, however.

The combined influence of n and f on the uniform and total strain is illustrated in Fig. 8(*c*). Both uniform and total strains decrease with increasing imperfection size. The amount of drop in uniform strain increases with the value of n itself, and the spread between uniform and total strain also shrinks in a similar manner. For imperfection size of ~0.006, even the total strain falls short of the n value.

Combined Influence of n and m

It has been shown that the presence of m does not influence the uniform strain significantly but affects the post-uniform portion of the engineering stress-strain plot. Figure 9 shows plots of post-uniform strain as a function of m for $n = 0.05$, 0.10 and 0.20. It is interesting to note that the increase in post-uniform strain produced by n alone (for $m = 0$) is enhanced many times as m increases. On the other hand, the effect of m is complimented well by larger values of n. Thus the combined influence of n and m is significantly greater than that of either n or m alone.

Influence of Constitutive Law

Figure 10 shows the influence of using Eq. [17b] in comparison to Eq. [17a] for the same values of $n = 0.2$ and $m = m' = 0.01$. It must be emphasized that $m' = 0.01$ means a slightly higher rate sensitivity than $m = 0.01$. In spite of this, however, Eq. [17b] affects load equilibrium in such a manner as to produce slightly smaller elongation than Eq. [17a] suggests. It is clear that the test rate influences only the load level if Eq. [17b] is operative. In case of Eq. [17a] both uniform and total elongations might be affected by test rate as well as the level of load.

COMPARISON WITH THE BIFURCATION THEORY

Bifurcation theory has been used in studies of necking in circular cylindrical specimens.[8-10] This theory relates the change from a purely uniform deformation mode to a nonuniform one to the change in the slope of stress-strain curve. It predicts that the necking (diffuse) strain for a specimen with fixed grip ends is the same as the strain at maximum load, while the necking strain is somewhat greater for a specimen with shear-free ends.[9] Even though it appears nearly impossible to pinpoint the diffuse necking strain experimentally, the above references suggest that the difference between the strains for necking and maximum load is strongly influenced by yield strain, specimen geometry and n value. No experimental corroboration of either of these effects or similar effects on the load-extension plots (be-

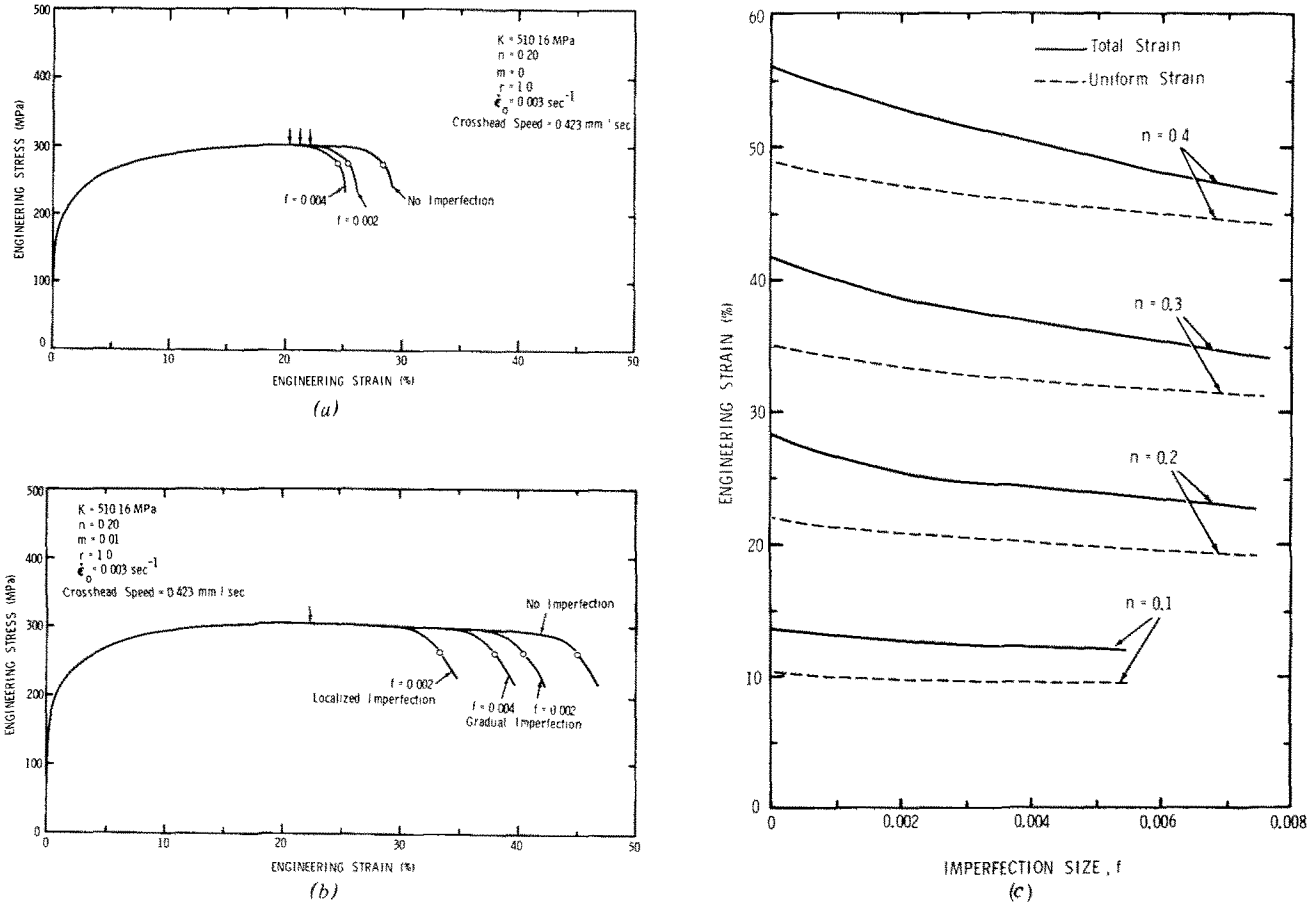

Fig. 8—Engineering stress-strain curves calculated for (*a*) three different imperfection sizes (0, 0.002 and 0.004) for the case of $n = 0.2$ and m = 0, (*b*) three different imperfection sizes (0, 0.002 and 0.004) for the case of $n = 0.2$ and m = 0.01. The vertical arrows indicate the maximum load position and the open circles in the decreasing load part of the curves correspond to the discontinuance of deformation at a node 1.27 mm from the specimen center. An additional calculation is also shown for a localized imperfection of the type as in Fig. 3 (size = 0.002), situated not over the entire 27.94 mm but over the central 4 elements (5.08 mm) on either side of the specimen center. (*c*) Plots of uniform and total strains over 50.8 mm gage length are shown as function of specimen imperfection size for the type of imperfection shown in Fig. 3. The results are for different values of $n = 0.1$, 0.2, 0.3 and 0.4. Elongations up to the point of the open circle (as in Figs. 7 and 8) are considered only.

yond the maximum load) has been reported. In the present work, the strain at maximum load was found to equal n, for a perfect specimen with gripped ends, which is what would be expected on the basis of bifurcation theory. Detailed comparison of load-extension plots from the present analytical results could not be made, however, since this has not been worked out using the bifurcation theory.

An aspect of the present model, apparently more realistic than others, is that the change from a uniform state of deformation to a nonuniform one does not occur at a single instant, but through a gradual discontinuance of straining from the specimen fillet region. Small degree of strain nonuniformity is present even before maximum load and therefore, the definition of a diffuse neck and its exact point of occurrence become arbitrary. Recent work on the bifurcation analysis of sheet specimens[11] actually predicts that a large number of bifurcation modes are possible even before the load maximum. This view is somewhat closer to the concept of gradual development of a nonuniformity. The remaining challenge is thus an understanding of the load-extension plot beyond maximum load. In the experimental results to be presented for various sheet materials (as well as those in Ref. 1), the differences in these plots (for identical specimen geometry and yield strains) are not explicable in terms of their n values; the influence of strain-rate sensitivity, zero, positive or negative, must be included to completely understand these.

COMPARISON WITH EXPERIMENTAL RESULTS

To test the analytical model with real material behavior, tensile tests were conducted on the following materials: 1) aluminum-killed steel, 2) rimmed steel, 3) 70 : 30 brass, 4) 2036-T4 aluminum (Al-2.7 pct Cu) alloy and 5) 5182-0 aluminum (Al-4.0 pct Mg) alloy. E-8 specimens were pulled at 1 cm/min and n, K, r, and m parameters were determined. n and K values in Eq. [17a] are obtained respectively, from the slope and intercept (at $\epsilon = 1$) of log (true stress) *vs* log (true strain) plots. r values, *i.e.* the ratio of width-to-thickness strains, are obtained from measurements of deformed grids on the specimens (Fig. 1(*b*)) prior to the load maximum. The strain-rate sensitivity parameters, m, are determined from changes in crosshead speed during a test. The stress differential, $\Delta\sigma$, from strain rates of $\dot{\epsilon}_1$ to $\dot{\epsilon}_2$, is used

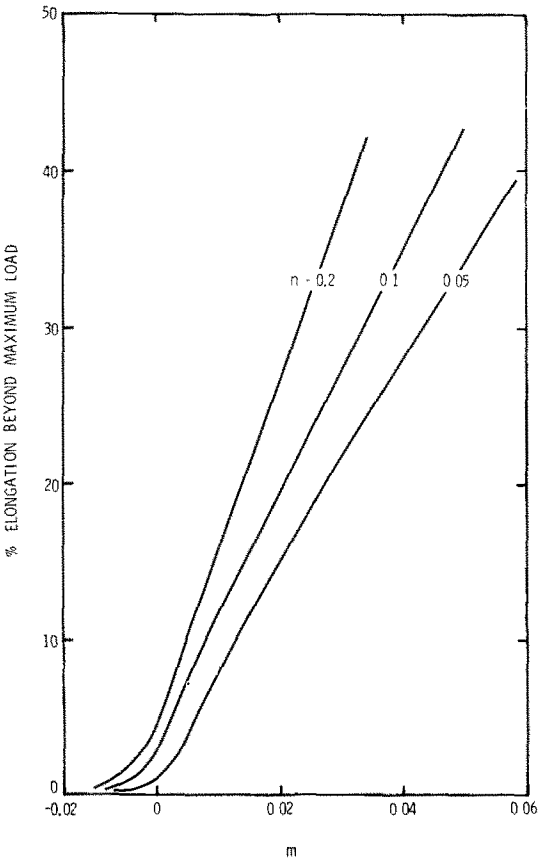

Fig. 9—Percent elongation over 50.8 mm gage length beyond maximum load, (or postuniform elongation) is plotted as a function of m for three different values of n = 0.05, 0.1 and 0.2. Elongations up to the point of the open circle (as in Figs. 7 and 8) are considered only.

to calculate m, using the relationship: $m = \Delta\sigma/\ln(\dot{\epsilon}_2/\dot{\epsilon}_1)$

Figures 11(a) to (e) compare the experimental engineering stress-strain curves with calculated ones for the various materials. For both aluminum-killed and rimmed steels, the agreement is excellent. Analysis does not simulate the behavior at low strain levels very closely since the actual n-values for these materials are lower at these strain levels. In case of brass (Fig. 11(c)), the best fit value of n (= 0.54) over the entire strain range produces reasonable agreement of most of the curve, however, calculated uniform and total strains are much larger than the observed values. It is well known that brass and certain aluminum alloys have a significantly lower value of n near the maximum load.[1] Based on the measured terminal value of n (= 0.46), the calculated curve matches the experimental results quite well near the maximum load. As expected, however, this worsens the fit for the lower strain region on the curve. The input of a strain-dependence of n into the analysis will be required therefore for a closer fit over the entire strain range.

Figure 11(d) shows a similar result for 2036-T4 aluminum, using the terminal value of n (= 0.18). Again a larger value of n can best describe the early part of the curve, while a lower n describes the last part better. It is interesting to note that the serrations in the engineering stress-strain plot around and beyond the maximum load have been appropriately predicted from the negative value of m (= −0.0025).

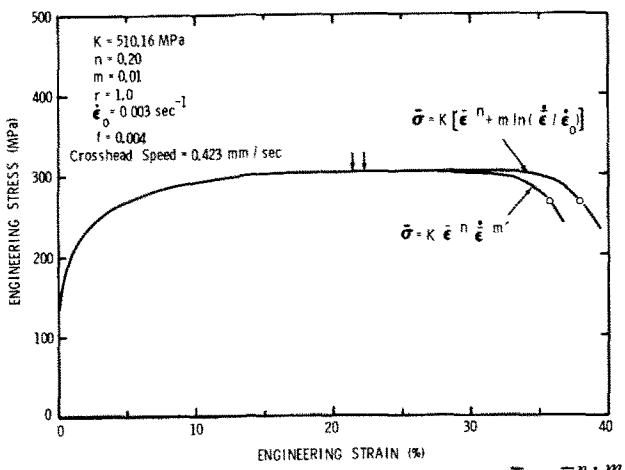

Fig. 10—The influence of the constitutive laws, 1) $\bar{\sigma} = K\bar{\epsilon}^{n}\dot{\bar{\epsilon}}^{m'}$ and 2) $\bar{\sigma} = K[\bar{\epsilon}^{n} + m' \ln \dot{\bar{\epsilon}}/\dot{\epsilon})]$, on the engineering stress-strain curves is shown for n = 0.2 and $m = m'$ = 0.01.

This effect was found to result from periodic increase and decrease in strain rates in the elements of the specimen. The amplitude and frequency of these serrations are, however, different from those observed, probably because the strain increments used in computation were much too coarse to resolve such details.

While the uniform strain is not influenced by m = −0.0025 in the case of 2036-T4 aluminum, a larger negative m of −0.007 in the case of 5182-0 aluminum (Fig. 11(e)) not only reduced the uniform and total strains from their expected values, but shifted the onset of serrations to much smaller strains. This agrees with the observed behavior, except for the amplitude and frequency of serrations. Like the previous two materials, a smaller value of terminal n also exists for this material. The important conclusion here is that a sufficiently negative m can actually reduce the uniform strain to a value lower than n.

SUMMARY AND CONCLUSIONS

A rigid/plastic constitutive relation including power law strain hardening and strain-rate hardening has been used to model the deformation in a sheet tensile specimen. A finite difference computation procedure simulates the progressive cessation of deformation starting from elements in the fillet region toward the minimum section (in the center) of the specimen, thereby generating a strain peak. This gradual strain localization is more realistic than the abrupt mode change in the bifurcation theory, and explains large postuniform extensions. Good agreement has been obtained between experimental and calculated engineering stress-strain curves for a variety of materials, particular emphasis having been given to the extension beyond maximum load. Some general conclusions regarding the deformation process and influences of various material and geometric parameters are listed below:

1) The strain-rate in the minimum section increases from the onset of deformation in two stages. It reaches an extremely rapid rate of increase near $\epsilon_x = n$ (for materials with m = 0), which coincides with the discontinuance of deformation in all fillet

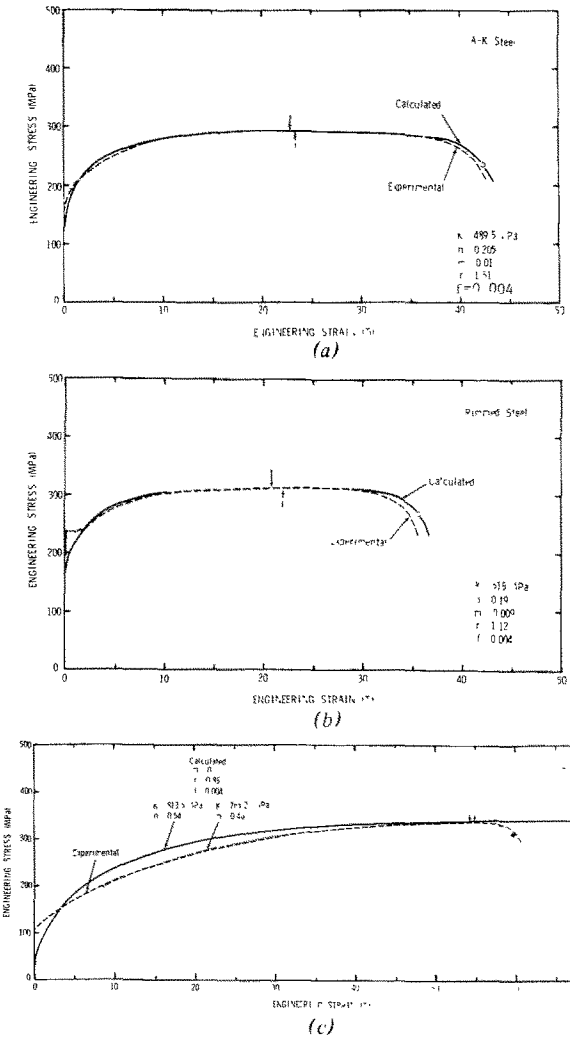

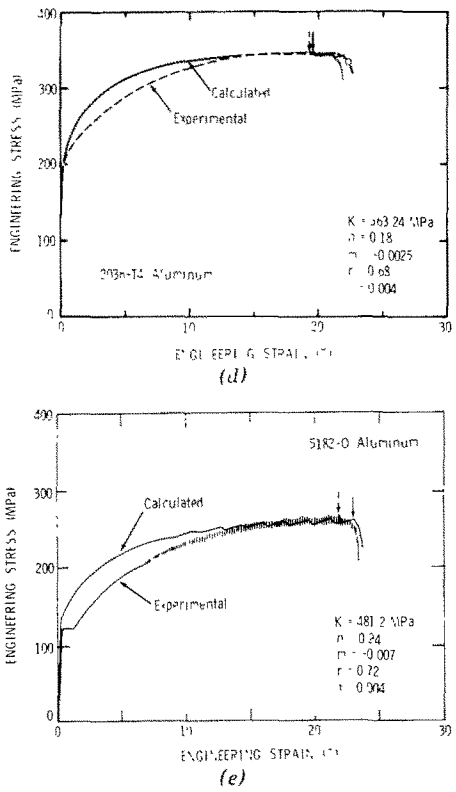

Fig. 11—Comparison of experimental and calculated engineering stress-strain cuves for (*a*) aluminum-killed steel, (*b*) rimmed steel, (*c*) 70-30 brass—two calculations were carried out, one on the basis of $n = 0.54$ for low strains, and the other on the basis of $n = 0.46$ for strains near maximum load, (*d*) 2036-T4 aluminum—the calculation is based on the value of n that best fits near the maximum load, (*e*) 5182-0 aluminum—the calculation is based on the value of n that best fits the near maximum load.

elements. The second stage consists of strain localization within the gage length with another rapid rise in strain rate, up to nearly two orders of magnitude. The presence of a small positive m (~0.01) reduces the rate of increase, and thereby shifts the transition strain (from first to the second stage of rate increase) to a larger value.

2) The stress-ratio (σ_y/σ_x) developed in a sheet tensile specimen is generally very small ($\sim 10^{-4}$) and increases only slightly with deformation. The greatest increase, however, is near the minimum section where it reaches about 10^{-1} before failure.

3) A cosine-shaped imperfection in the width dimension (to simulate specimen taper) was studied. Imperfections of small size ($\Delta w/w_0 \sim 0.004$) reduce uniform strains unless m is positive. However, a larger drop occurs in postuniform strain: for example, in the case of $n = 0.20$ and $m = 0.01$, postuniform strain drops by 7 pct when imperfection size reaches ~0.004. Localized imperfection is substantially more detrimental than a gradual tapering imperfection of the same size.

4) Both uniform and postuniform strains increase with increasing n, the increase in postuniform strain being within 1.5 to >4 pct upon an increase in n from 0.05 to 0.40.

5) The most dramatic effect comes from the presence of small positive m. Uniform strain increases slightly (~1 pct) from the presence of a positive m, however, postuniform strain increases from 3 pct to 43 pct due to an increase of m from 0 to 0.05. The combined influence of n and m is substantially larger than those of n or m alone. For example, an $m = 0.02$ can produce 27 pct postuniform strain when $n = 0.2$, as against only 15 pct when $n = 0.05$. A sufficiently negative m can reduce both uniform and total strains significantly and produce serrations in engineering stress-strain plot. The strain for the onset of serrations decreases with more negative values of m.

6) An increase in r increases postuniform strain slightly. This increase is somewhat enhanced by the presence of a positive m. A change of r from 1 to 2 in the case of $n = 0.20$ and $m = 0.01$ increases postuniform strain by ~3 pct.

REFERENCES

1. A K Ghosh Accepted for publication in the Journal of Engineering Materials and Technology, *Trans ASME*, July, 1977
2. A K Ghosh *Met Trans*, vol 5, 1974, p 1067
3. E W Hart: *Acta Met*, vol 15, 1967, p. 351
4. A K. Ghosh and R. A. Ayres: *Met Trans. A*, 1976, vol 7A, p. 1589
5. W. C Chen *International Journal of Solids and Structures*, vol 7, p. 685, 1971.
6. A S. Argon, J Im, and A Needleman. *Met. Trans. A*, vol. 6A, 1975, p 815
7. N N Davidenkov and N I Spiridonova *Proceedings of the American Society for Testing Materials*, vol 46, p 1147, 1946
8. J P Miles *J Mech Phys. Solids*, vol 19, 1971, p 89.
9. A Needleman *J Mech Phys. Solids*, vol 20, 1972, p. 111
10. J W Hutchinson and J P Miles *J Mech Phys Solids*, vol. 22, 1974, p. 61.
11. R. Hill and J. W. Hutchinson *J Mech Phys Solids*, vol 23, 1975, p 239.